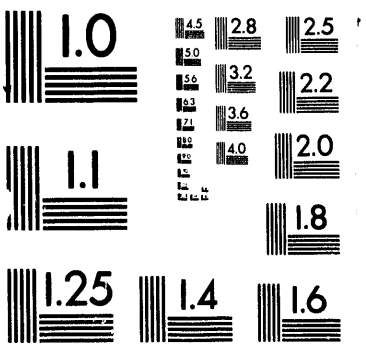
1.0
1.1
1.25
1.4
1.6
1.8
2.0
2.2
2.5
2.8
3.2
3.6
4.0
4.5
5.0
5.6
6.3
7.1
8.0
9.0

1 of 1

CONF-9310164--6

LA-UR- 93-3588

Title: The Effects of Proton Beam Quality on the Production of Gamma Rays for Nuclear Resonance Absorption in Nitrogen

Author(s): R. E. Morgado, C. C. Cappiello, M. P. Dugan, C. A. Gould ng, S. D. Gardner, C. L. Hollas, B. L. Berman, R. W. Hamm, K. R. Crandall, J. M. Potter, and R. A. Krauss

Submitted to: SPIE Conference
October 5-8, 1993
Innsbruck, AUSTRIA

MASTER

DISTRIBUTION OF THIS DOCUMENT IS UNLIMITED

Los Alamos
NATIONAL LABORATORY

Los Alamos National Laboratory, an affirmative action/equal opportunity employer, is operated by the University of California for the U.S. Department of Energy under contract W-7405-ENG-36. By acceptance of this article, the publisher recognizes that the U.S. Government retains a nonexclusive, royalty-free license to publish or reproduce the published form of this contribution, or to allow others to do so, for U.S. Government purposes. The Los Alamos National Laboratory requests that the publisher identify this article as work performed under the auspices of the U.S. Department of Energy.

Form No. 836 R5
ST 2629 10/91

The effects of proton beam quality on the production of gamma rays for nuclear resonance absorption in nitrogen

R. E. Morgado, C. C. Cappiello, M. P. Dugan, C. A. Goulding, S. D. Gardner, and C. L. Hollas

Los Alamos National Laboratory, Los Alamos, NM 87545

B. L. Berman

George Washington University, Washington, DC 20052

R. W. Hamm, K. R. Crandall, and J. M. Potter

AccSys Technology, Inc., Pleasanton, CA 94566

R. A. Krauss

Federal Aviation Administration, Atlantic City International Airport, NJ 08405

ABSTRACT

We describe a method for performing nuclear resonance absorption with the proton beam from a radio frequency quadrupole (RFQ) linear accelerator. The objective was to assess the suitability of the pulsed beam from an RFQ to image nitrogen relative to that of electrostatic accelerators. This choice of accelerator results in tradeoffs in performance and complexity, in return for the prospect of higher average current. In spite of a reduced resonance attenuation coefficient in nitrogen, we successfully produced three-dimensional tomographic images of real explosives in luggage the first time the unoptimized system was operated. The results and assessments of our initial laboratory measurements are reported.

1. INTRODUCTION

In an earlier program[1], we established the feasibility of an explosives detection approach based on nuclear resonance absorption in nitrogen[2]. Nitrogen in explosives simulants were imaged using gamma rays produced by low-current, DC proton accelerators from the $^{13}C(p, \gamma)^{14}N$ reaction. We concluded then that practical applications of the technique to airport security would require proton currents in the 5 to 15 mA range. The radio frequency quadrupole (RFQ) linear accelerator used in this project was acquired by Los Alamos National Laboratory (LANL) and partially upgraded by AccSys Technology, Inc.[3] with the support of the US Federal Aviation Administration (FAA)[4]. The objective was to assess the suitability of the pulsed beam from an RFQ to image nitrogen relative to that of electrostatic accelerators. Although the central issues were beam emittance and pulse structure, other consideration included beam stability, size, cost and complexity. This choice of accelerator has led to trade-offs in performance and complexity, in return for the prospect of higher average current. In this paper we describe our method for producing the gamma rays for nuclear resonance absorption with an RFQ accelerator and present the results and assessments of our initial laboratory measurements.

This FAA-sponsored project has been a collaboration between LANL and the Soreq Nuclear Research Center (SNRC), Yavne, Israel. Each collaborator developed a variant of a resonance absorption explosives detection system with the LANL accelerator as the common gamma-ray source. This paper describes the LANL effort to characterize the accelerator; both the SNRC and LANL detection systems are addressed in companion papers.

1.1 Physical basis for the gamma-ray production concept.

The basis of the technique is the existence of a narrow energy state in the nucleus of ^{14}N that results in a strong resonance in the photo nuclear cross section for the reaction $^{14}N(\gamma, p)^{13}C$ at 9.17 MeV[5,6,7]. Gamma rays are absorbed by nitrogen, followed by the prompt emission of a proton and a ^{13}C nucleus. The transition rate from the ground state of ^{14}N is unusually large, and, as a result, 9.17-MeV gamma rays are strongly absorbed, resulting in a strong indication of the presence of nitrogen.

The essential feature of our approach is the use of the inverse reaction[8], $^{13}C(p, \gamma)^{14}N$, to produce the gamma rays at the resonance energy. A 1.75-MeV proton beam incident on ^{13}C produces gamma rays at the resonance energy within a

narrow angular interval with respect to the proton beam direction. As a result, desirable system characteristics are achieved: a fan beam, localized source of gamma rays of the correct energy; a low level of radiation with no residual radioactivity, thus minimizing shielding; an efficient, inorganic scintillator detectors is sufficient; and required proton currents are attainable by current accelerator technology.

The technique is distinguished by the narrowness of the resonance, its large integrated cross section (absorption probability), and its uniqueness to nitrogen, all of which result in high detection sensitivity and insensitivity to backgrounds. The 9.17-MeV gamma rays are very penetrating in ordinary matter, making it difficult to shield the explosives from detection. The technique is similar to x-ray imaging, but with notable exceptions: the image is of nitrogen alone; the probing radiation is very penetrating to all other elements; and overlying clutter that complicates the interpretation of conventional x-ray images is removed, simplifying the interpretation of the image and allowing for the possibility of automated detection.

1.2 Technical approach

The gamma rays relevant to nuclear resonance absorption in nitrogen are those within the very narrow band of energies (~125 eV) defined by the total width of the 9.17-MeV resonance. We have investigated two sources of production: the bremsstrahlung beam from an electron accelerator and the inverse resonance reaction with the beam from a proton accelerator. The former required the development of gamma-ray detectors capable of operating in the intense backgrounds of a pulsed electron accelerator. Attempts to model and measure bremsstrahlung beams indicated the practical difficulties of this approach. We determined early on that the proton source is technically advantageous and we have directed our subsequent attention to this source.

The gamma-ray yield from the $^{13}C(p, \gamma)^{14}N$ reaction as a function of proton energy is described by the Breit-Wigner form of the cross section,

$$\sigma(E_p) = \pi \lambda_p^2 \; g \; \Gamma_\gamma \Gamma_p \; / [(E_p - E_R)^2 + (\Gamma_t / 2)^2], \qquad (1)$$

where g = statistical factor, Γ_i = partial widths for channel i, Γ_t = total resonance width, λ_p = proton wavelength/2π, and E_R = the proton resonance energy. The cross section is integrated analytically, and the gamma-ray yield determined for a target density, n atoms/cm^3, rate of energy loss, dE/dx, and total energy loss, ΔE. The maximum, thick-target yield in γ/proton is

$$Y_{max}(\infty) = (\pi/2)\, n \; \sigma_{max} \; \Gamma_t \; / \; [(dE/dx)_E] \qquad (2)$$

where $\sigma_{max} = 4\pi \lambda_p \, g \; \Gamma_\gamma \Gamma p \; / \Gamma_t^2 =$ 89.4 mb . The thick-target yield of 9.17-MeV gamma rays is then

$$Y_{max} (\infty) = 0.63 \times 10^{-8} \; \gamma\text{/proton into } 4\pi. \qquad (3)$$

The gamma-ray yield is the limiting factor in any practical application with currents presently available from proton accelerators. To generate a useful fluence for airport applications, average proton currents from 5 to 15 mA were indicated, based on calculations, measurements, and several analytical models of detection and imaging systems.

1.3 Accelerator considerations

Specifications for the proton beam were derived from measurements by LANL and SNRC on electrostatic accelerators. We concluded at that time that conventional DC accelerator technology did not appear able to produce the average currents for an operational system. RFQ technology, developed in recent years, had met and exceeded our projected requirements, at least for instantaneous current. Higher average currents would require increasing the rf and beam duty factors of existing RFQ accelerators.

Besides proton current, there are other considerations for a resonance absorption source. In addition to contributions from the natural width of the resonance and Doppler broadening[9], the angular interval over which resonance gamma rays are emitted in the laboratory is broadened further for several reasons: the emittance of the proton beam is finite, (the angular divergence, transverse beam extent, and the energy spread about the mean proton kinetic energy), and the practical thickness of the production target produces multiple scattering. Useful currents would be that fraction of the proton beam that met the emittance as well as the intensity requirements for resonance absorption.

DEC 13 1993
OSTI

1.4 Operational objecticves and accelerator specifications.

The laboratory test was designed to duplicate, as nearly as possible, the beam characteristics that would be encountered in an operational system. The specifications for the RFQ developed for the purpose of our laboratory tests are listed in Table I. An existing low-duty-factor accelerator, originally designed and constructed for another purpose, was acquired from AccSys Technology, Inc. of Pleasanton, CA, and partially upgraded to meet the minimum requirements for our laboratory tests. The major limitations to achieving higher average currents with this system were considered to be the available RF power and the cooling capacity of several system components. The final specifications were a compromise between what was deliverable within the available time and resources of the program.

Table I
The nominal specifications for the modified AccSys Model PL-2 RFQ accelerator

ION SOURCE & INJECTOR		RFQ ACCELERATOR	
output current (peak)	30 mA	acceptance (normalized)	1.0 p mm-mrad
normalized output emittance	0.5 p mm-mrad	transverse space charge limit	60 mA
hydrogen gas flow	1.0 sccm	intervane voltage	63.2 kV
		cavity rf power (w/o beam loading)	165 kW
RF AMPLIFIER		beam pulse width	20-25 ms
		beam pulse repetition rate (nominal)	500 Hx
operating frequency	425 MHz	beam energy spread (90%)	<+ 12 keV
maximum output power	240 kW	maximum peak current	25 mA
maximum duty factor	0.025	average output current	500 mA

2. RESONANCE GAMMA-RAY PRODUCTION SYSTEM

2.1 Radio frequency quadrupole accelerator system

The AccSys Model PL-2 Radio Frequency Quadrupole (RFQ) linear accelerator is shown in Figure 1. The major accelerator subsystems include a 30-kV H+ ion source and injector, a 1.75-MeV RFQ linear accelerator and auxiliary components, main rf power amplifier system, computer control and monitoring system, and an energy debuncher cavity and rf power system.

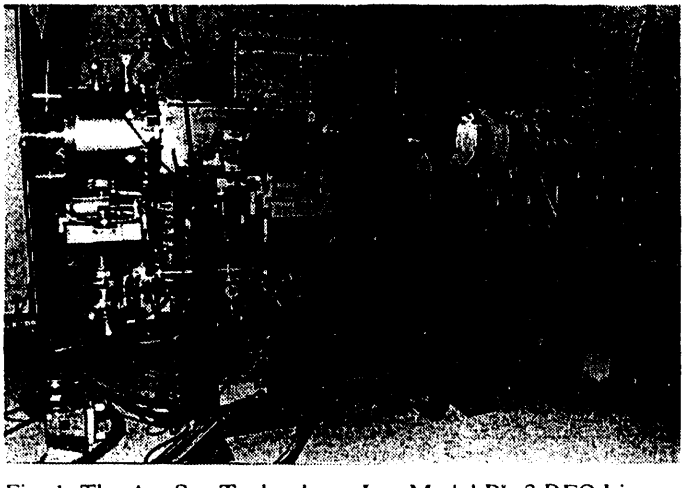

Fig. 1. The AccSys Technology, Inc. Model PL-2 RFQ Linear Accelerator.

2.1.1 Ion source and injector

A duoplasmatron ion source with a single-gap, spherically-converging extraction geometry, generates and accelerates the injected proton beam to 30 keV. An oxide-coated, bifilar, nickel gauze filament, operated at 150 W, provides the electron emission for establishing the hydrogen plasma. The plasma is focused through an extraction aperture into a self-biased plasma expansion cup, from which the proton beam is extracted. The ion source and injector are biased to 30 kV relative to the grounded extraction electrode. The 30 keV H+ and a small fraction of H_2+ ions are focused onto the RFQ aperture with a two-gap electrostatic einzel lens.

2.1.2 RFQ linear accelerator

The RFQ linear accelerator is a four-vane resonator fabricated from copper-plated, extruded aluminum. The patented geometry uses four captured rf seals between four identical cavity quadrants, each sinusoidal-modulated

to produce a longitudinal accelerating field. The adiabatically-introduced modulations capture more than 80% of the dc injected beam and has an inherently high current capability. The structure is designed to resonate at 425 MHz and accelerates 30 keV protons to 1.75 MeV in a distance of 1.6 m with an rf surface field gradient of 35 MV/m. The resonator is mounted within a stainless steel vacuum envelope that is easily aligned to the high-energy beam transport system.

2.1.3 Main RF power amplifier

For pulsed output currents of 25 mA, approximately 210 kW of peak rf power is required to drive the resonator through a single rf loop positioned at its midpoint. Power is supplied by a four-stage, AccSys 240 kW rf amplifier with parallel planar triode tubes. The crystal oscillator, timing and protection circuits, and the phase, amplitude, and frequency feedback control circuits are located in the low-level rf chassis, which also supplies the power and timing signals for the energy debuncher system, described below. The final amplifier stage contains twelve planar triodes operated in the grounded-grid configuration, with parallel outputs but individual dc and cathode-bias circuits. Protection circuits crowbar the stored energy through an ignitron switch in the event of sparking. DC-to-rf conversion efficiency is greater than 50% at a maximum average output of 6 kW.

2.1.4 Monitoring and control

The AccSys Instrumentation Monitoring and Control Unit (IMCU) operates the injector, the accelerator vacuum system, and the main rf amplifier through a PC-based control system. IMCUs located in each subsystem control and monitor the active functions and parameters, as well as the interlock status and timing of the units. Feedback loops in the injector and main rf amplifier are hard-wired circuits, but with the operational-loop set points under computer control. A watchdog timing circuit insures that computer control of all subsystems is maintained at all times.

2.1.5 Energy Debuncher

In order to meet the energy resolution specification, an energy debuncher cavity is introduced. The energy spread inherent in the high-current beam pulses causes the protons in the individual microbunches to separate longitudinally as they pass through the beam transport system. After the protons have separated a calculated amount, a single-gap rf cavity is used to reduce the energy spread by decelerating the faster protons in the leading edge of the pulse, and accelerating those in the trailing edge, while those at the mean energy are unperturbed. The energy debuncher also introduces a means to vary the energy of the beam over a limited range, approximately + 20 keV around the mean energy. The single-gap cavity is powered by a small rf amplifier driven by low-level driver of the main rf amplifier. Frequency feedback is established with a motor-driven slug tuner in the cavity to maintain it at the same operating frequency as the RFQ resonator.

2.2 High-energy beam transport system

The high-energy beam transport system (HEBT), designed and instrumented by LANL, performs several important functions: it transports the beam from the RFQ accelerator to the production target, matching the conditions for full transmission with the specified magnification; it provides debunching to reduce the energy spread in the beam; and it redirects the beam from the horizontal to the vertically downward direction, permitting the resonance absorption imaging to be performed in a nearly-horizontal plane, which greatly simplifies the tomographic inspection.

2.2.1 Beam elements

The HEBT elements include a permanent magnet quadrupole (PMQ), a quadrupole doublet (Q1 and Q2), the single rf-cavity energy debuncher, and the Danfysik 90-degree bending magnet (BM) with shaped, focusing pole faces. The proton beam emerges from the RFQ resonator converging in the x-z plane and diverging in the y-z plane, where z is along the axis of the proton beam and x and y are orthogonal axes in the plane perpendicular to the beam axis. The PMQ was positioned immediately downstream of the RFQ structure where it can focus the diverging component of the beam while leaving the converging component relatively unaffected. Q1 and Q2 produce an approximate double waist at the center of the energy debuncher, so that the cross section of the beam is small, insuring a uniform electric field over the region of the applied rf. Q1 and Q2 also simultaneously prepare the beam to match the emittance requirements of the bending magnet. Element (BM) bends the beam 90 degrees vertically downward while simultaneously providing focusing in both horizontal and vertical planes. An elevation view of the vertical HEBT is depicted in Figure 2.

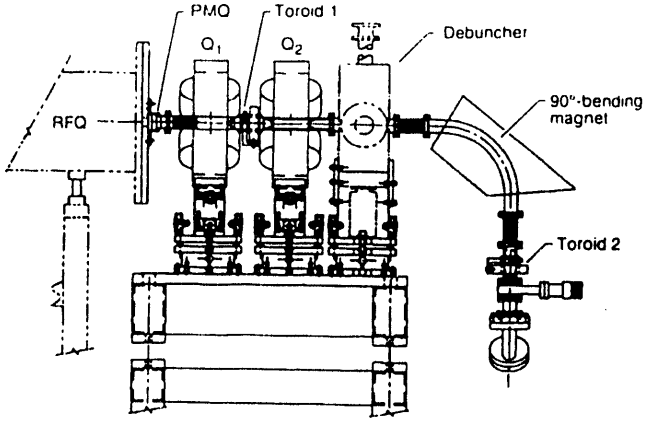

Fig. 2. Vertical HEBT elevation view.

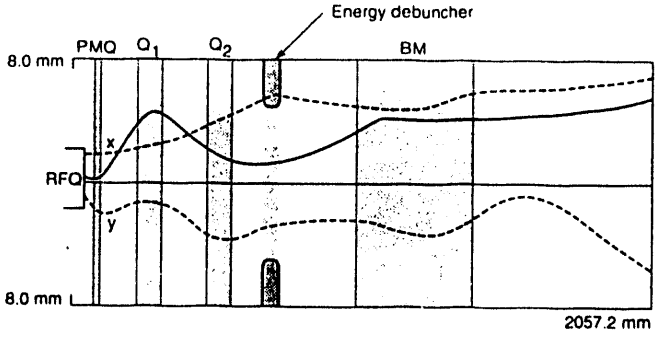

Fig. 3. TRACE-3D beam envelope of vertical HEBT design calculation.

2.2.2 Beam design

The constraints on the beam transfer matrix included the formation of a quasi-double waist at the location of the single rf cavity of the energy debuncher, the preparation of the beam emittance to match the acceptance of the bending magnet, and the formation of the final image at the gamma-ray production target with the correct magnification, divergence, and energy spread. The only tunable elements in the beam line were Q1, Q2, and the phase difference between the accelerator and the energy debuncher rf pulses, once the drift distances and the pole face angles of the bending magnet had been specified. The beam design program TRACE-3D10, modified to include space-charge effects and a single-gap rf cavity, was used to design the beam optics. The calculated TRACE-3D ray traces of the beam envelope in the x-z, y-z and E-z dimensions are depicted in Figure 3.

2.2.3 Beam instrumentation

The time-structure and emittance of the beam from a low-duty factor RFQ accelerator, together with the space-charge effects of a high peak-current ion source, add to the complexity of achieving and maintaining the required beam characteristics over useful periods of operation. To assure that the beam requirements were met, the relevant beam parameters were monitored on a continuous basis. These included the maintenance of the beam transverse dimensions, the beam centroid position, the mean proton energy, and the energy spread. Beam monitoring elements included current transformers, a profile monitor, and a charge integrator on the target.

2.2.3.1 Beam profile monitor

The transverse dimensions of the proton beam at the target are important for several reasons. For practical considerations, beam power dissipation in the water-cooled target requires that the beam current be distributed over a maximum area, while optical requirements of the imaging system make a small focal spot size desirable. An additional requirement involves monitoring beam position drifts over time which are due to instabilities in the beam transport elements and which result in an apparent enlargement of the focal spot size. A National Electrostatics Corporation beam profile monitor was inserted upstream of the gamma-ray production target. Although intended for operation in low-current DC beams, we were able to successfully operate it in our low-duty factor accelerator. Because of our low-duty factor, any single rotation of the profile monitor secondary emission wire through the beam resulted in a sampling of points along the beam profiles. To generate complete profiles, sampling over many beam pulses was required. A long-persistence oscilloscope was used to display the profiles and the accelerator repetition rates were selected to avoid harmonics of the profile monitor rotational frequency.

2.2.3.2 Target current and charge monitors

Pearson current transformers, with a sensitivity of 0.5 mV/mA, were positioned in the HEBT between Q1 and Q2 and at the exit of BM to measure transmission. The proton current on target was determined by electrically isolating the target assembly with an insulating spacer and measuring the voltage generated by the beam current across a 50 ohm resistor to ground. All current signals were monitored continuously at the operator console. For charge normalization, target current was integrated with a Brookhaven National Laboratory Current Integrator.

3. MEASUREMENTS AND ASSESSMENTS

Characterization measurements were performed at the AccSys Technology, Inc. facility and, after disassembly, shipping, and reassembly, at Los Alamos National Laboratory. Operating conditions differed substantially between the two locations. These included barometric pressure, ambient temperature, and the commissioning of a new HEBT to deflect the beam vertically down. Ambient summer temperatures at the Los Alamos installation often exceeded 35 °C during operations, providing unintended but extreme tests of all system components. Large diurnal temperature variations were recorded and additional cooling to maintain stability was not always available. Radio frequency tuning and phasing were particularly affected by temperature variations and the measured results reflected the effects of thermal variations in our performance assessments.

3.1 Accelerator parameters

3.1.1 Ion source and injector

Operation of the ion source and injector at the higher elevation (2100 m) of the laboratory facility at Los Alamos introduced corona discharges and sparking that were not observed at sea level. To prevent damage to sensitive components due to the large voltage transients that accompany sparking, additional protective circuitry was developed and implemented.

3.1.1.1 Peak source current, Ip

The duoplasmatron source and injector, nominally rated at 30 mA peak current, achieved the specified peak current of 25 mA at the 2.5% duty factor level only during factory testing. The injected current pulse was measured by a Pearson current transformer positioned in the injector, upstream of the einzel lens. Nominal injected peak currents achieved in Los Alamos ranged between 16 and 20 mA, depending on the conditions of the ion source filament and the plasma expansion cup aperture. This lower peak current is close to the space-charge limit at which the energy debuncher is effective in reducing the energy spread. This peak current was maintained by frequent retuning. Eventual replacement of the complete ion source assembly after installation at Los Alamos did not improve the output and the source of the problem is still under review.

3.1.1.2 Filament lifetime

The rated lifetime of the oxide-coated, bifilar nickel gauze filament is nominally 1000 hours. Measured lifetimes in this system were less, closer to 100 hours, with the ion source output usually degraded to an unacceptably low level. Expansion cup apertures were replaced when ion source pressures rose due to erosion of the aperture, attributable primarily to inadequate cooling for this low duty factor ion source.

3.1.1.3 Stability

Accelerator output was interrupted by frequent sparking in the einzel lens assembly of the injector. The problem was diagnosed as the result of low-energy beam halo striking the einzel lens during the beginning and end of each pulse, charging it to high voltage, at which point a spark occurred. The lens voltage was pulled to ground potential and injected beam was interrupted for several seconds while the power supply re-established the operating voltage. Once a spark was initiated, the process repeated itself two to three times per minute, resulting in interruptions of output and unpredictable beam conditions. Evidence of carbonized tracking along the insulators of the lens support assembly confirmed the diagnosis. After the tracks were removed, the incidence of sparking was greatly reduced for the remaining measurements. The ion source arc current and the injected current wave forms are depicted in the top oscilloscope traces of Figures 4 and 5.

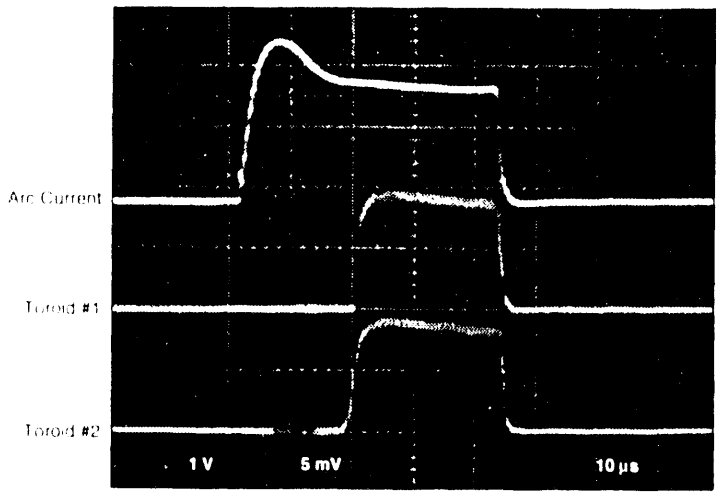

Fig. 4 Ion source arc current and toroid waveforms

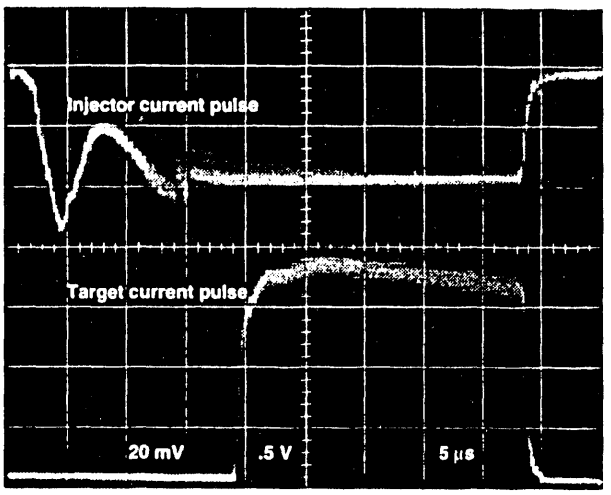

Fig. 5 Injector and target current transformer waveforms

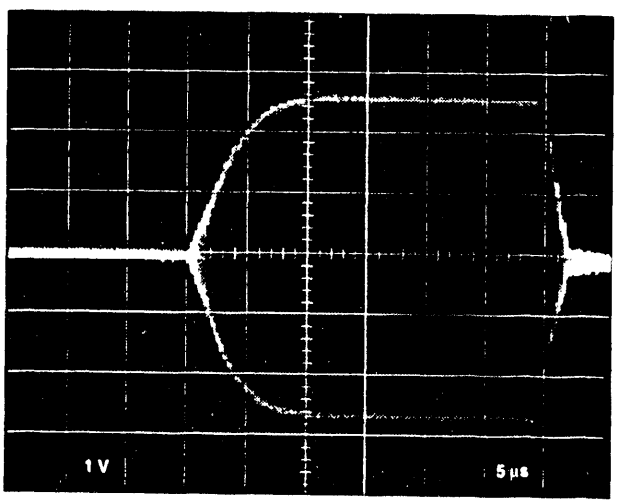

Fig. 6 Main RF envelope waveform

3.1.2 RFQ beam

3.1.2.1 Time structure and duty factor

The specified beam duty factor of 2.5% was achieved during acceptance testing at the AccSys Technology facility with a 50 ms beam pulse at 500 Hz. After reassembly at Los Alamos, the highest attained duty factor was 2%, limited primarily by the tripping off of the rf power supply by protective circuitry due to fault conditions and sparking in the einzel lens caused by the high pulse-repetition rate. Stable operating conditions were established and maintained at two different combinations of pulse width and pulse repetition rate: 20 ms at 600 Hz, and 45 ms at 300 Hz, resulting in duty factors of 1.2 and 1.4%, respectively. Current transformer wave forms for the high-energy beam are depicted in Figures 4 and 5. The main rf pulse envelope is depicted in Figure 6.

Despite intense counting rates as a result of the peak current and pulse structure of the beam, the detectors and data acquisition system developed for the demonstration and used for the beam characterization measurements performed gamma-ray spectroscopy with little degradation in energy resolution. This system is described more completely in an accompanying paper.

3.1.2.2 Average beam current

A maximum average current of 600 mA was reached at the factory acceptance testing, and 500 mA was produced over 8 hours, with no unscheduled breakdowns of the equipment but with a number of interruptions due to real and spurious faults in the rf protection circuitry and sparking in the einzel lens. After reassembly in Los Alamos, the maximum average current achieved under any condition was 350 mA. For continuous operation during data acquisition for imaging, average

current on target was limited to 250 mA . The reduced average current added additional time to all measurements and this contributed an element of non-reproducibility to the results due to instabilities.

3.1.2.3 Mean proton energy and energy resolution

The mean proton beam energy and energy spread were determined initially with Rutherford back scattering and nuclear resonance gamma-ray excitation. In the former measurement, a thin gold foil on carbon was used to elastically scatter protons. A measurement of the component scattered at 90 degrees from each element provided a relative beam energy measurement of better than 2 keV.

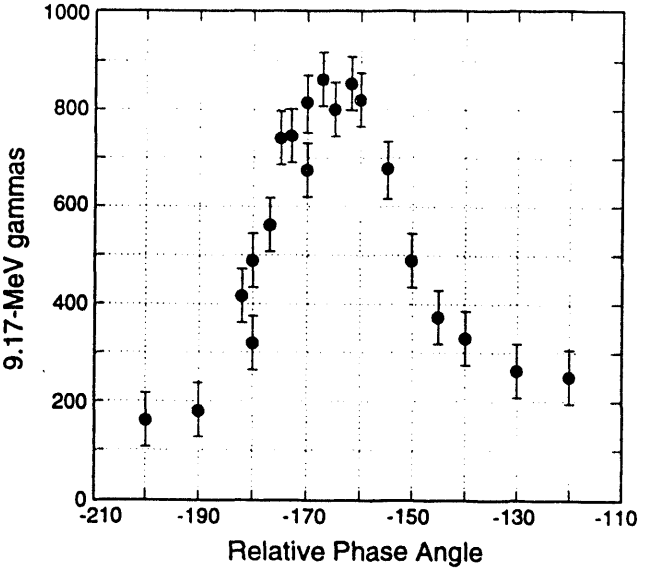

Fig. 7. $^{13}C(p,\gamma)\ ^{14}N$ RFQ excitation curve.

The excitation curve measurements for the $^{13}C(p, \gamma)^{14}N$ determined both the mean energy and the energy spread in the beam. The excitation curve for a 160 mg/cm carbon target as a function of rf phase difference between the accelerator and the energy debuncher rf power is depicted in Figure 7. The leading edge is a measure of the energy spread in the proton beam, while the width of the plateau and the known target thickness are used to calibrate the relative phase angle of the abscissa in terms of proton kinetic energy. The energy spread at the target, with the energy debuncher optimized, was + 6 keV FWHM, in agreement with the beam design calculations . By employing a target that was thicker than the beam energy spread and by operating within the plateau of the excitation curve, small, slow drifts in proton energy could be accommodated without loss of gamma-ray output.

3.2 High-energy beam transport parameters

3.2.1 Tuning and alignment

The beam elements were carefully aligned optically and magnetically to insure the centering of the beam axis. Quartz viewers were used at reduced duty factor to visualize the beam position and transverse dimensions. Beam tuning proceeded one element at a time to maximize transmission and alignment and to minimize beam steering as each magnetic element was tuned over its range of field values.

3.2.2 Energy stability and resolution

The mean proton beam energy and energy resolution were controlled by the relative rf phase difference and pulse amplitude of the rf pulse applied to the energy debuncher. Both the rf phase difference and amplitude were determined by maximizing the output of 9.17-MeV gamma rays from a thin carbon target. Frequent detuning of the relative rf phase difference between the main rf and the energy debuncher occurred without warning, either due to temperature variations or problems in the feedback loop circuitry. This introduced large energy spreads in the beam with an associated reduction in gamma-ray output. Corrections were made to the feedback loop circuitry in the rf phase control, but the situation continued intermittently due to a mechanical problem with the servo-driven slug tuner of the energy debuncher cavity.

The y dimension of the beam at the target was a sensitive measure of the energy spread and, hence, of the effectiveness of the energy debuncher, since the dispersion introduced by the bending magnet was magnified at the target. Observations of increases in the y dimension at the target were inevitably traced to a problem in the slug tuner feedback loop.

3.2.3- Beam spot on target

The transverse beam dimensions in the x-z and y-z planes were measured with a quartz window during the beam tuning phase. With the calculated current settings for Q1 and Q2, the beam at the target was a 1-cm diameter circular spot,

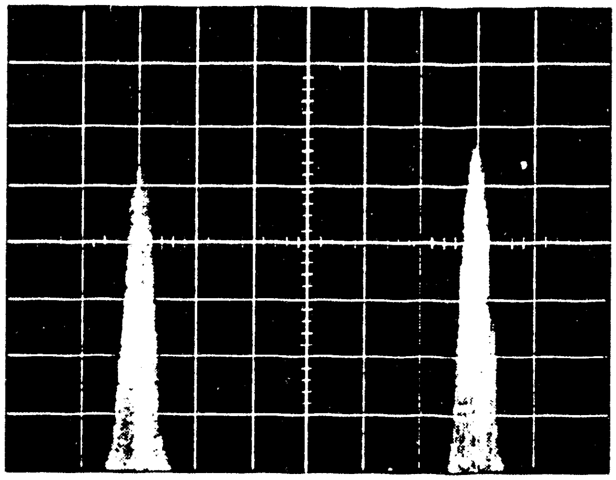

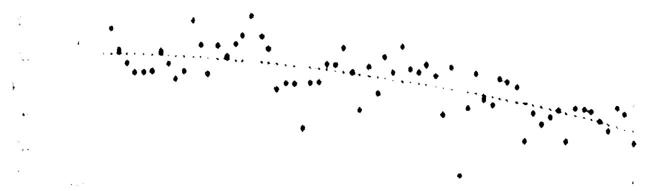

[illegible]

as predicted. The beam spot on the target was monitored during extended operations with the beam profile monitor, but at higher average currents, heating damage to the profile monitor occurred. Subsequently, the beam profile monitor could only be used sparingly, reducing the overall monitoring effectiveness. The measured x and y beam profiles are shown in Figure 8. The measured FWHM of the beam in both the x and y dimensions is [illegible] 6 mm, in good agreement with the beam design calculation which required 90% of the beam intensity within a 1 cm diameter spot.

3.2.4 Beam divergence and transmission

The beam divergence at the gamma ray production target was specified at < 8 mrad in both the x-z and y-z planes. A design tune of the HEBT was found that satisfied the specifications. During the initial tuning of the HEBT, a 10% beam loss was observed at the entrance aperture of the vacuum tank of the bending magnet, the result of an oversight in the specification of the bending magnet gap to accommodate the vacuum tank thickness. The potential for excessive heating and damage to the vacuum tank at higher average currents necessitated an alternative HEBT tune, but a tune that minimized the beam loss and simultaneously satisfied the overall beam constraints could not be found. A compromise tune minimized the transmission loss but produced a large beam divergence in the y-z plane at the production target. The overall effect was to reduce the net resonance absorption coefficient, particularly in those detectors in the imaging array that were located closer to the y-z beam plane. This effect is illustrated in Figure 9 in which the measured absorption in a thin (~4 g/cm² of nitrogen) sample of melamine is plotted as function of detector position relative to the beam central axis.

3.3 Resonance absorption parameters

3.3.1 Gamma ray yield

The yield of 9.17 MeV gamma rays at the plateau of the thick target excitation curve was measured with a well characterized 3 in. x 3 in. BGO detector. The yield was consistent with the predictions of Eq. 3, corrected for solid angle and detection efficiency and normalized to the proton charge on target. Reductions in the gamma ray output with time in the multi-element thin target caused by [illegible] were not measurable at the average currents available for extended periods of operation.

3.3.2 Resonance angle determination

A resonance absorption [illegible] was measured in liquid nitrogen by a detector and [illegible] located on a vertical [illegible]. The [illegible] resonance absorption [illegible] occurred at the same angle [illegible] the vertical [illegible] beam.

3.3.3 Nuclear resonance attenuation determination

The net nuclear resonance attenuation was measured in a sample of liquid nitrogen. The detector and collimator assembly were positioned approximately 1m from the production target on the vertically-adjustable translating mechanism of the tomographic imaging system. The collimator slit subtended an angular opening of 0.7 degrees. The measured net nuclear resonance absorption integral curve is depicted in Figure 10. The non-nuclear component of the total absorption has been approximated by simultaneously measuring the attenuation of the 6- and 7-MeV gamma rays from the $(p,\alpha\gamma)$ reaction in ^{19}F.

The effective nuclear resonance absorption mass attenuation coefficient for nitrogen was measured to be 0.015 cm^2-g-1. Allowing for the difference in collimator sizes, this result falls short of the 0.025 - 0.028 cm^2-g-1 value measured on electrostatic accelerators. The reduced attenuation is manifested in a reduction in the contrast sensitivity in the tomographic images. No systematic attempt to study this discrepancy were permitted in the time frame of the present phase of the work, although several possible sources are mentioned in the following section.

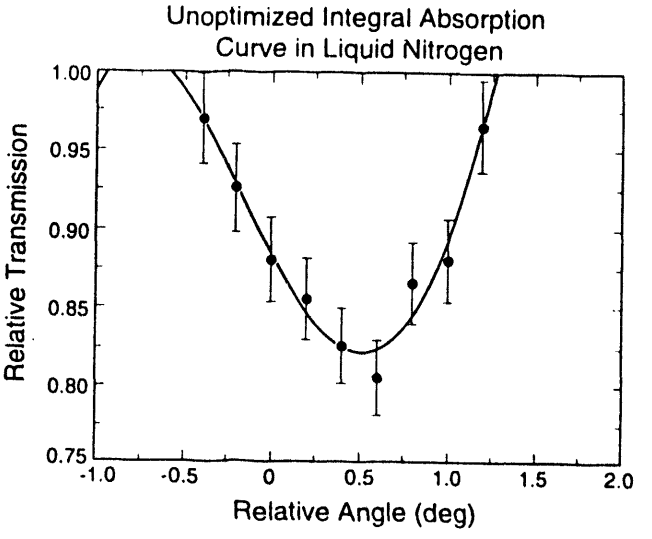

Fig. 10. Resonance absorption integral curve in liquid nitrogen.

4. CONCLUSION

Our initial attempt to perform nuclear resonance absorption with the proton beam from an RFQ accelerator has been described. Technical and practical problems remain to be solved prior to deployment in the field. The problems associated with this system were diagnosed and we have identified the areas where future improvements can be made. These include the design of more robust ion injector components and rf power systems and the inclusion of additional cooling capacity for the entire accelerator system. Our experience clearly revealed the inadequacy of the einzel lens for high average current pulsed accelerators. Alternative methods exist for performing the same function in a future design. System performance is summarized in Table II.

Table II

Measurements and Assessments Summary

Parameter	Specification	Measured	Assessment
Peak current (mA)	25	16-18	[illegible]gnosed ion source problem
Filament lifetime (hr)	1000	< 100	Inadequate cooling of ion source
Beam Pulse Width (ms)	20 - 50	20 - 45	Within specifications
Repetition Rate (Hz)	500	250	Einzel lens sparking, RF faults
Beam Duty Factor (%)	2.5	1.2 - 1.4	Einzel lens sparking, RF faults
Average Current (mA)	500	250	Einzel lens sparking, RF faults
Beam Energy (MeV)	1.747	1.747	Within specifications
Tunable Range (keV)	+ 20	+ 20 keV	Within specifications
Energy Spread (keV)	+ 12	+ 10 keV	Within specifications
x-z divergence (mrad)	+ 5	<+ 5	Within specifications
x-y divergence (mrad)	+ 5	>+ 10	HEBT tune
mass attenuation coeff.(cm2/g)	-	< 0.02	divergence, alignment, DE, DQ unoptimized

The smaller measured nuclear resonance mass attenuation coefficient in nitrogen has the net effect of reducing the contrast in our images, making the reconstruction and interpretation of the nitrogen tomographs less definitive. We had neither the time nor resources to study the effect as a function of the suspected beam parameters. The expedient and reasonable course at the time was to accept the tradeoff in reduced attenuation and push on. Possible sources of this degradation have been identified and include effects that can be attributed to accelerator performance and to unrelated factors. Effects directly attributable to the accelerator and beam transport include the observed large beam divergence, variable beam output and energy stability, and a possibly excessive energy spread at the production target. Other factors include the alignment of the resonance absorption system and the particular technique selected for correcting for the non-resonant absorption component. We feel confident that proper attention to these important details will improve the overall performance of future systems. We are encouraged by our results in which an unoptimized system, nevertheless, produced three-dimensional tomographic images and detected explosives the very first time it was operated.

5. REFERENCES

1. "The Feasibility of Detecting FAA-Threat Quantities of Explosives in Luggage and Cargo Using Nuclear Resonance Absorption in Nitrogen", Phase I Final Report, Los Alamos National Laboratory, Advanced Nuclear Technology, Internal Report (October 1989).

2. Goldberg, M. B. Vartsky, D., et. al., Informal Proposal, Soreq Nuclear Research Center, Yavne, Israel, December 1985.

3. AccSys Technology, Inc., 1177 Quarry Lane, Pleasanton, CA 94566.

4. Federal Aviation Administration, FAA Technical Center, Aviation Security R&D Service, Atlantic City, NJ.

5. Hannah, S.S. and Meyer-Schutzmeister, Luise, "Resonant Absorption by the 9.17-MeV Level in 14N", Physical Review 115, 4, (1959).

6. Biesiot, W. and Smith, Ph. B., "Parameters of the 9.17-MeV Level in 14N ", Physical Review C 24, 6, (1981).

7. Vartsky, D., Goldberg, M. B., Engler, G., Goldschmidt, A., Breskin, A., Morgado, R. E., Hollas, C. L., Ussery, L.E., Berman, B. L., and Moss, C. E., "The Total Width of the 9.17-MeV Level in 14N", Nuclear Physics A505 (1989) 328-336.

8. Seagrave, John D., "Radiative Capture of Protons by 13C", Physical Review 85, 2, (1952).

9. Flusberg, A., Science Research Laboratory Internal Memorandum, March 1993.

10. Crandall, K. R., "TRACE-3D Documentation", LA-UR-90-4146 (December 1990).

DISCLAIMER

This report was prepared as an account of work sponsored by an agency of the United States Government. Neither the United States Government nor any agency thereof, nor any of their employees, makes any warranty, express or implied, or assumes any legal liability or responsibility for the accuracy, completeness, or usefulness of any information, apparatus, product, or process disclosed, or represents that its use would not infringe privately owned rights. Reference herein to any specific commercial product, process, or service by trade name, trademark, manufacturer, or otherwise does not necessarily constitute or imply its endorsement, recommendation, or favoring by the United States Government or any agency thereof. The views and opinions of authors expressed herein do not necessarily state or reflect those of the United States Government or any agency thereof.

DATE
FILMED
2/8/94
END